

Experimental Investigation on Box-Wing Configuration for UAS

Experimental Investigation on Box-Wing Configuration for UAS.

Authors: Barcala, M*, Cuerno-Rejado, C. **, del Giudice, S. *, Gandía-Agüera, F.*, Rodríguez-Sevillano, A.A.*.

* *E.U.I.T. Aeronáutica, Universidad Politécnica de Madrid, Madrid, Spain.*

** *E.T.S.I. Aeronáuticos, Universidad Politécnica de Madrid, Madrid, Spain.*

miguel.barcala@upm.es, cristina.cuerno@upm.es, fernando.gandia@upm.es, angel.rodriguez.sevillano@upm.es

ABSTRACT

The range for airframe configurations available for UAS is as diverse as those used for manned aircraft and more since the commercial risk in trying unorthodox solutions is less for the UAS manufacturer. This is principally because the UAS airframes are usually much smaller than the manned aircraft and operators are less likely to have a bias against unconventional configurations.

One of these unconventional configurations is the box-wing, which is an unconventional solution for the design of the new UAS generation. The existence of two wings separated in different planes that are, however, significantly close together, means that the aerodynamic analysis by theoretical or computational methods is a difficult task, due to the considerable interference existing. Considering the fact that the flight of most UAS takes place at low Reynolds numbers, it is necessary to study the aerodynamics of the box wing configuration by testing different models in a wind tunnel to be able to obtain reasonable results.

In the present work, the study is enhanced by varying not only the sweepback angles of the two wings, but also their position along the models' fuselage. Certain models have shown being more efficient than others, pointing out that certain relative positions of wing exists that can improve the aerodynamics efficiency of the box wing configuration.

BIOGRAPHIES

Dr. Barcala M. Ingeniero Técnico Aeronáutico (Bachelor), Ingeniero Aeronáutico (Master) and PhD by Universidad Politécnica de Madrid, Madrid, SPAIN. Head of E.U.I.T. Aeronáutica, Chairman of the Management Committee El Aeronáutica y del Espacio and Professor at Departamento de Aerotecnia, Universidad Politécnica de Madrid, Madrid, SPAIN.

Dra. Cuerno-Rejado C. Ingeniero Aeronáutico (Master) and PhD by Universidad Politécnica de Madrid, Madrid, SPAIN. Associate Professor at Departamento de Vehículos Aeroespaciales, Universidad Politécnica de Madrid, Madrid, SPAIN.

Mr. Del Giudice, S. Ingeniero Técnico Aeronáutico (Bachelor) by Universidad Politécnica de Madrid, Madrid, SPAIN.

Prof. Gandía-Agüera, F. Ingeniero Técnico Aeronáutico (Bachelor). Ingeniero Aeronáutico (Master) by Universidad Politécnica de Madrid, Madrid, SPAIN. Associate Professor at Departamento de Aerotecnia, Universidad Politécnica de Madrid, Madrid, SPAIN.

Prof. Rodríguez-Sevillano, A.A. Ingeniero Técnico Aeronáutico (Bachelor). Ingeniero Aeronáutico (Master) by Universidad Politécnica de Madrid, Madrid, SPAIN. Associate Professor at Departamento de Aerotecnia, Universidad Politécnica de Madrid, Madrid, SPAIN.

Research areas: Airplane Conceptual Design; Low Reynolds number aerodynamics, Preliminary Design of Unmanned Aerial Vehicles, Rotary Wing Aircrafts, High Speed Trains aerodynamics.
Lectures areas: Aerodynamics of Aircrafts and Wind Energy, Flight Mechanics, Rotary Wing Aircrafts, Aircraft Design; End of Degree Projectwork for Bachelor Aerospace Engineering degree.

Nomenclature

C_L	Lift coefficient
C_D	Drag coefficient
C_M	Pitching moment coefficient. C_M is calculated, in any case, referred to fixing axis model.
C_L/C_D	Lift to drag ratio. Aerodynamic efficiency
α	Angle of attack referred to box-wing zero lift line
V	Mean wind speed on wind tunnel test section (m/s)
S	reference wing area (m^2). In all cases, is the total wing area (the upper plus the lower wing area).
c	Mean geometrical wing chord (m)
L	Lift (N)
D	Drag (N)
M	Pitching moment (N.m)
$Re = Vc/\nu$	Reynolds number
ν	kinematic viscosity of air (m^2/s)
r	UAV reference

Introduction

In order to reduce the over-increasing fuel costs and CO₂ emissions of transport airplanes, the designers are reconsidering different unconventional configurations that were proposed and discarded many years ago (1). This effort is also being developed due to the fact that the conventional configuration is approaching its limit in productivity and capacity at a size around that of the Airbus A380 (2).

A number of configurations have been proposed in the past (3), which can be indentified in terms of two variables: the number and position of lifting-surfaces (canard, tandem, classical, three-surface, joined-tips and tailless) and the solution selected for allocating the payload (one/two fuselages, partially inside the fuselage and the wing, and completely in the wing). By the combination of one of each variable, there is a different aircraft configuration.

Among those possible configurations obtained in the previously described procedure, a special interest is paid nowadays to the lay-outs in which the lifting surfaces (typically wing and horizontal tailplane) are connected. The most general configuration in this category is the called "box-wing". This shape reaches the maximum possible reduction in induced drag by means of connecting the wing tips to the stabilizer tips through some vertical elements. The original idea was proposed by Prandtl in 1920 (4) and it is being reconsidered nowadays also under the name of Prandtlplane (5). Prandtl found that the biplane has a lower drag than an equivalent monoplane and its minimum drag is obtained when the two wings of the biplane have the same span. Further on, more induced drag reduction can be achieved if wing end-plates are attached to the wingtips, thus making a closed system (box). In a very simplified way, this effect is due to the fact that the presence of the wingtips causes a reduction in the net induced velocity in the downwash of each wing. Hence, the induced angle of attack is

decreased for the same total lift, reducing the induced drag which is proportional to the magnitude of the induced velocities in the downwash (11).

For civil transport airplanes, when performing cruise conditions, induced drag contributes to 43% of the total drag during cruise flight (5). Talking about UAS, which usually have lower aspect ratio, that percentage may be higher. In this work, the box-wing configuration is being analyzed for an unmanned air vehicle in the mini-category, by means of an experimental research.

Nevertheless, the box-wing configuration has been employed in a small number of existing UAV. The oldest project was the North-American Alliant Techsystems RQ-6 Outrider, delivered by the US Army and cancelled after some flights. The Alliant RQ-6 Outrider was an Advanced Concept Technology Demonstrator (ACTD). The project started in 1995 and finished in 2003 when the specification of being a common flight platform meeting the requirements of the US Army, Navy and Marine Corps at the same time was unsuccessful. Also, the Hammerhead (an amateur project from the Oklahoma State University) has the same configuration. Both RQ-6 and Hammerhead employ what is called as the positive stagger, which means that the aerodynamic center of the forward (and higher) wing is ahead the aerodynamic center of the rear (and lower) wing.

There are, also, some other UAV developed in the box-wing configuration but fixing the wings system with negative stagger. In this category, the models found are the D-1, from Dara Aviation; the short-range Roadrunner UAV project, from the French company ATE; the IKELOS Project, developed by a joint team composed by the Virginia Polytechnic Institute and State University and the Loughborough University; and the tactical UAV project FrontLine V-STAR from Frontline Aerospace Inc.

UAVs are inducing quite significant changes in software for design optimization, consequently an investigation is needed on the way to merge, the shape, the mission, the payload (7) and certain aerodynamic parameters (8), in order to meet the present-day demands for airworthiness requirements. This work is enhanced with the experience of the authors in the area of design and construction of UAVs for civil applications, for both fixed and rotary wings. In the UAV design and manufacturing areas, they have supervised a group of students to design and build a real UAV; in that sense, the following paper can be consulted (9). Other universities present similar activities carried by undergraduate students.

Having in mind the predicted drag reduction of the box-wing layout, the research team from UPM decided to investigate the real possibilities of employing this unconventional configuration for the design of a long-endurance mini UAV. The research work is centered, in a first phase, in an experimental investigation of the aerodynamic characteristics of this configuration using a wind tunnel. Therefore the objective of this work is to obtain a characterization of the aerodynamic force coefficients for two Reynolds numbers and four different models representing a box-wing shaped mini UAV.

Models description

As it was stated in the previous section, in order to define the models' geometry, a real UAV configuration was selected based on data from the existing unmanned negative staggered box-wing shaped airplanes. The UAV selected was the D-1 model, developed by Dara Aviation. The D-1 manufacturers claim for a lightweight structure (25 kg) being capable of

allocating up to 10 kg payload and reaching a range of 1500 km, for a payload of 4 kg. The selection of this model has been based, mainly, in its simplicity helping in the models' manufacturing process, which is published elsewhere (6).

Figure 1 depicts the planform of the first four models built and tested. The model labeled BW-1 is the reference model, which uses almost the same geometric proportions and sweep angle as the D-1 UAV. In order to investigate the effects of the wings interference, the models labeled BW-2, BW-3 and BW-4 share the same longitudinal position and sweepback angle for the front wing, while varying the longitudinal position for the root chord of the upper (rear) wing. In these models the root chord of the upper wing is moved gradually forward towards the front (lower) wing, until the sweepback angle for both wings reaches the same value (BW-4 model).

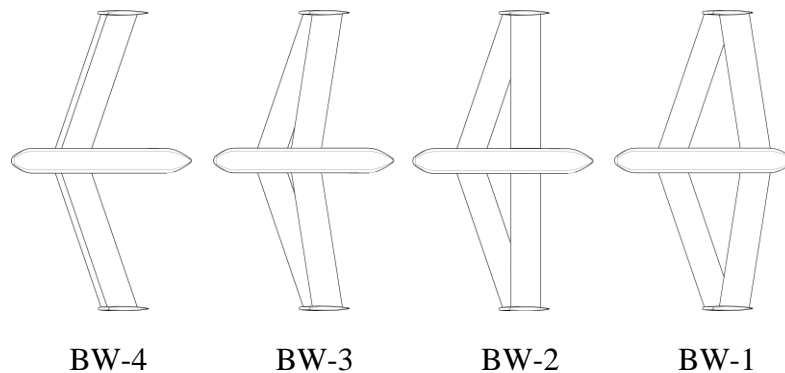


Figure 1.- Planform for the box-wing models. The position and sweepback angle for the front wing is the same, while the position of the root of the upper wing is varied.

Keeping in mind that the study is focused on documenting the interference between the two wings and how it varies, the airfoil selection was not a crucial factor in the model designing. In further research a rational selection of the most appropriate airfoil will be accomplished in order to optimize the aerodynamic results. Due, mainly, to the manufacturing methods an airfoil without double curvature was selected to facilitate the process. The airfoil finally chosen was the NACA 23012, which can be easily conformed in wood and it is very well documented in the open literature for a great range of Reynolds numbers. Half of the true model was built, being symmetric, in order to optimally make use of the E.U.I.T. Aeronáutica wind tunnel facilities. The chord of both wings is 5 centimeters, and the semispan of the wings is 25 centimeters. A table with all the relevant geometric data about the models is included in Table 1. The incidences of each wing (which difference is usually called *decalage* in the biplane theory) have been set equal to zero as a first step, based in the experimental results reported by Gall (11). In future work, this effect will be explored.





								
First Collection of Box wing models	BW-1		BW-2		BW-3		BW-4	
	Lower wing	Upper wing	Lower wing	Upper wing	Lower wing	Upper wing	Lower wing	Upper wing
Sweepback Λ (°)	18.9	-8.9	18.9	0	18.9	8.9	18.9	18.9
Distance from wing root to aircraft's nose (mm)	68	202	68	159	68	116	68	78

Table 1.- Box-wing models geometric data.

A second set of models, showed in Figure 2, was created in order to analyze the effect of the variation of the sweepback angles for the two wings at the same time. In these new seven models, the sweepback angle of the wings is modified while maintaining an unaltered distance midspan (distance between the wing roots and wing tips) and the airfoil of the previous models (NACA 23012). The first model (BW2-1) has an upper wing with no sweepback, and the angles varied until finally both wings were to stretch forward with a double negative sweepback (BW2-7). The models labeled BW1-1 of the first set is the same model labeled BW2-2 in the second set, and these are the reference model.

As in the first set of models, half of the true model was built, being symmetric. The chord of both wings is 5 centimeters, and the semispan of the wings is 25 centimeters like the models before. Table 2 collects all relevant geometric data for the new models.

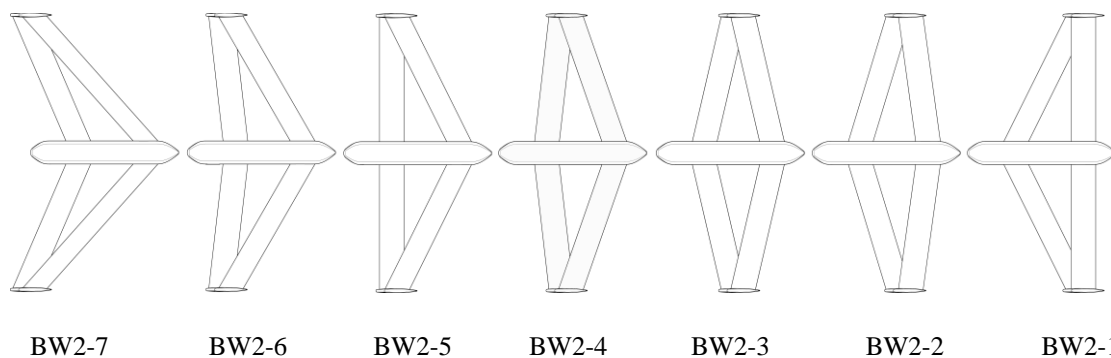


Figure 2.- Planform for the second set of box-wing models. The sweepback angle of the wings is modified while the distance between the wing roots and wing tips is unaltered.

Second set of box-wing models								
	BW2-1	BW2-2 = BW-1	BW2-3	BW2-4	Lower wing	Upper wing	Lower wing	Upper wing
Sweepback Λ ($^{\circ}$)	29.4	0	18.9	-8.9	14.7	-14.7	7.5	-21.5
Distance from wing root to aircraft's nose (mm)	68	202	68	202	68	202	68	202
	BW2-5	BW2-6	BW2-7		Lower wing	Upper wing	Lower wing	Upper wing
Sweepback Λ ($^{\circ}$)	0	-29.4	-7.5	-33.2	-22.9	-45.3		
Distance from wing root to aircraft's nose (mm)	68	202	68	202	68	202		

Table 2.- Second set of box-wing models geometric data.

Experimental Set-Up

The aerodynamics of several box-wing models is analyzed by testing each one in the wind tunnel N^o-1 of Departamento de Aeronautica (EUIT Aeronautica, Universidad Politcnica de

Madrid). This wind-tunnel is an open jet, low speed facility (Plint blower tunnel). The test section is 457×457 mm, and has a length of 1.200 mm. In order to ensure a longitudinal uniform pressure in the test section, boundary-layer correction is achieved by using corner fillets that extend along the contraction cone and the working section. The wind velocity profile at the model test section was uniform within $\pm 1\%$ and the mean turbulence intensity level being around 0,7%.

The aerodynamic forces on the aerofoil are measured using a three component Plint balance fitted to the wind-tunnel, that enables the lift, drag and pitching moments to be calculated. The three strain gages of the balance are connected to a calibrated digital readout that displays values of the forces (two vertical, fore and aft, and one horizontal, drag) in volts, and there are 3 different coefficients that need to be applied to convert these values into true forces (Newton) and moments (Newton per meter). Being correctly manipulated, the forces determined end up measuring lift, drag and pitching moment. This is a global procedure and therefore it is no possible to investigate the spanwise effects.

The test was performed at two different Reynolds numbers (70.000 and 140.000), $Re = Vc/v$, where V is the wind velocity in the test cross section, c the chord of the wing and v the kinematic viscosity of air and different angles of attack (from -8 degrees up to 25 degrees, degree by degree). The wind flow velocity in the test section was around 12,5 m/s and 25 m/s.

Having measured the necessary forces, and obtaining the non-dimensional aerodynamic coefficients, (C_L , C_D and C_M) the representation of these coefficients is the first step of the aerodynamics analysis of the box wing configuration and the UAV reference.

$$C_L = \frac{L}{1/2\rho V^2 S} \quad ; \quad C_D = \frac{D}{1/2\rho V^2 S} \quad ; \quad C_M = \frac{M}{1/2\rho V^2 S c}$$

An interesting aspect of the tests is seeing how the models behave once they reach stall conditions. To understand and analyze the phenomenon in a better way, tufts were strategically laid out on the wings and each angle of attack was also photographed to see where the stall began.

Wind tunnel corrections, like solid two dimensional blocking, wake blocking and streamline curvature were calculated using the classical method (10), but the main focus, in the present paper, wasn't to establish definitive quantitative values but to analyze change in forces behavior.

Experimental Results

Having obtained the non-dimensional aerodynamic coefficients, these coefficients were plotted as follows. The aerodynamics diagrams plotted were:

- The lift coefficient versus angle of attack (C_L vs α),
- the drag coefficient versus angle of attack (C_D vs α),
- the pitching moment coefficient versus angle of attack (C_M vs α),
- the aerodynamic efficiency versus angle of attack (C_L/C_D vs α) and the drag polar (C_D vs C_L).

These aerodynamic diagrams were plotted at $Re=70.000$ and $Re=140.000$ in the same figure to show the influence in these curves due to Re number.

The results obtained in this work have been compared with other experimental data (11) extracted from the scarce open literature available in which the box-wing configuration is studied in the low Reynolds number regime. The aerodynamic behavior exhibited by the reference BW-1 model for $Re = 140.000$ is comparable, from a qualitative point of view, to the characteristics of the model reported in the NASA model ($Re = 500.000$), especially in terms of lift-curve slope and maximum lift coefficient available. In the previously mentioned work (11), the maximum lift coefficient is 0,8 for $Re = 500.000$. In the present experimental work the maximum lift coefficient for the BW-1 model is 0,6, being the Reynolds number 3,6 times lower than the reported by Gall (11). This result is consistent with the reduction in the maximum lift coefficient reachable when Reynolds number decreases due to the increasing importance of the viscous effects.

In the figures from 3 to 8, symbols identify the box-wing model according to the following key: BW1-1 (squares), BW1-2 (rhombi), BW1-3 (triangles) and BW1-4 (circles). Open symbols corresponding to $Re=70.000$, and closed symbols corresponding to $Re=140.000$. In the figures from 9 to 14, symbols identify the box-wing model according to the following key: BW2-1 (asterisks), BW2-2 (squares), BW2-3 (rhombi), and BW2-4 (triangles), BW2-5 (circles), BW2-6 (x-cross) and BW2-7 (cross). Open symbols corresponding to $Re=70.000$, and closed symbols corresponding to $Re=140.000$.

Conclusions

An experimental research on several models of an UAV in box-wing configuration has been presented. The study has been centred in obtaining the main aerodynamic coefficients of two sets of box-wing models, tested in a low Reynolds number wind tunnel. The first set of models is composed of four configurations in which the front wing is unaltered while the root chord of the rear wing is moved gradually forward, until both wings have the same sweepback angle. In this set, both the higher C_{Lmax} and (C_L/C_D) at high angles of attack were obtained with the BW-1 model, while the changes in the low to medium angles of attack were quite small in all configurations.

The second set of models is composed of seven configurations in which the sweepback angle of both wings is varied, while the distance between the roots and tips of both wings is unaltered. In this set, the models BW2-2, BW2-3 and BW2-4 show the best characteristics, in terms of C_{Lmax} and (C_L/C_D) at high angles of attack. These models are, among the complete set, the ones in which the planform looks like a rhombus. One of the trends detected in the tufts visualization test (Figures 15 to 34) is that as the angle of attack is increased, the leading edge flow detachment in the front wing is delayed to higher angles of attack. Also, in the rear wing, the stall is produced for a higher angle than in the front wing. This behavior also justifies the appearance of the lift coefficient versus angle of attack curves.

Future Works: in order to deepen in the aerodynamic behavior of the box-wing configuration for low Reynolds numbers, it would be very valuable to carry-out a test campaign in a larger wind tunnel in which full-scale models could be tested. Also other geometric characteristics of the models will be considered. Parameters as the *decalage* (relation between front and rear incidence angles), airfoil family and twist variation law would be carefully optimized.

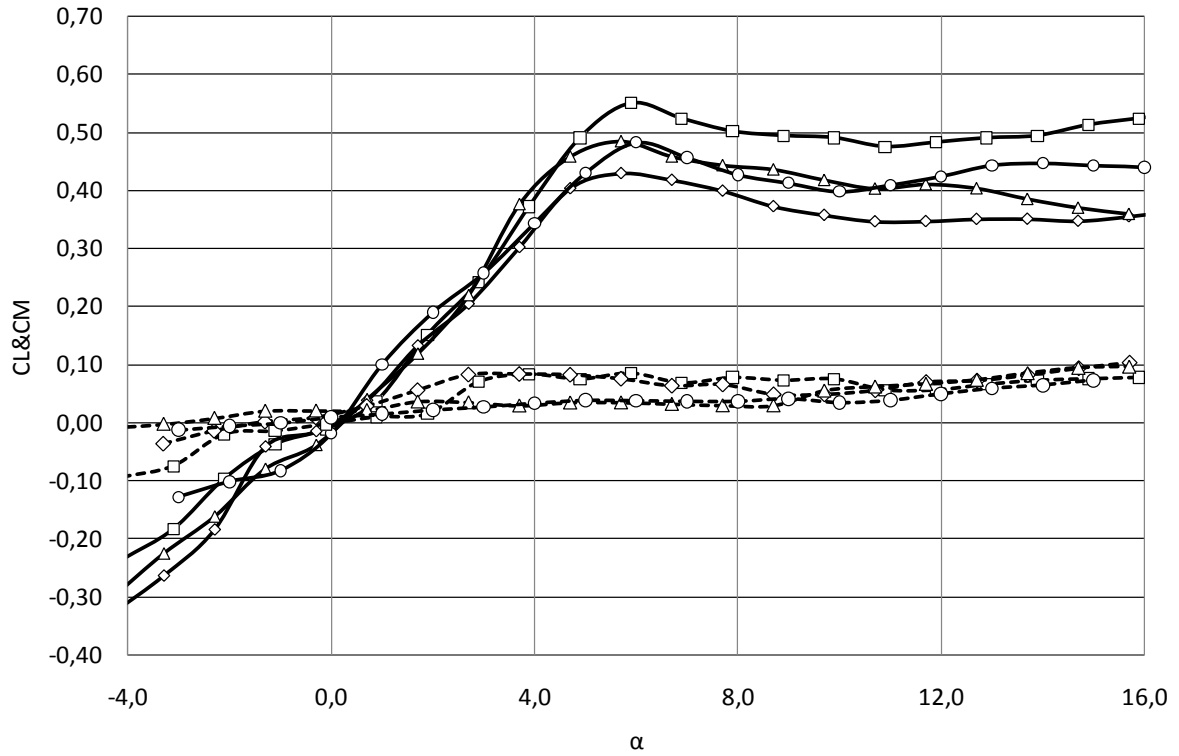


Figure 3.- Variation of lift coefficient (C_L) and pitching moment coefficients (C_M) versus angle of attack (α). The results correspond to $Re= 70.000$.

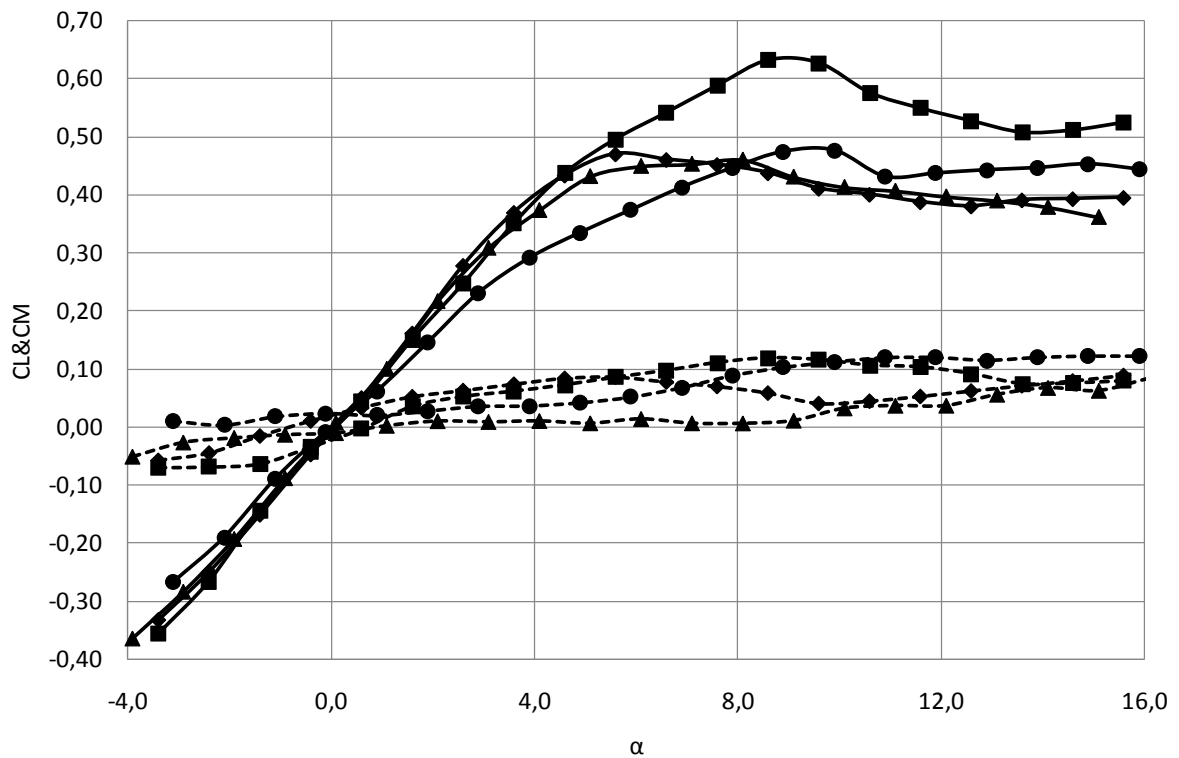


Figure 4.- Variation of lift coefficient (C_L) and pitching moment coefficients (C_M) versus angle of attack (α). The results correspond to $Re= 140.000$.

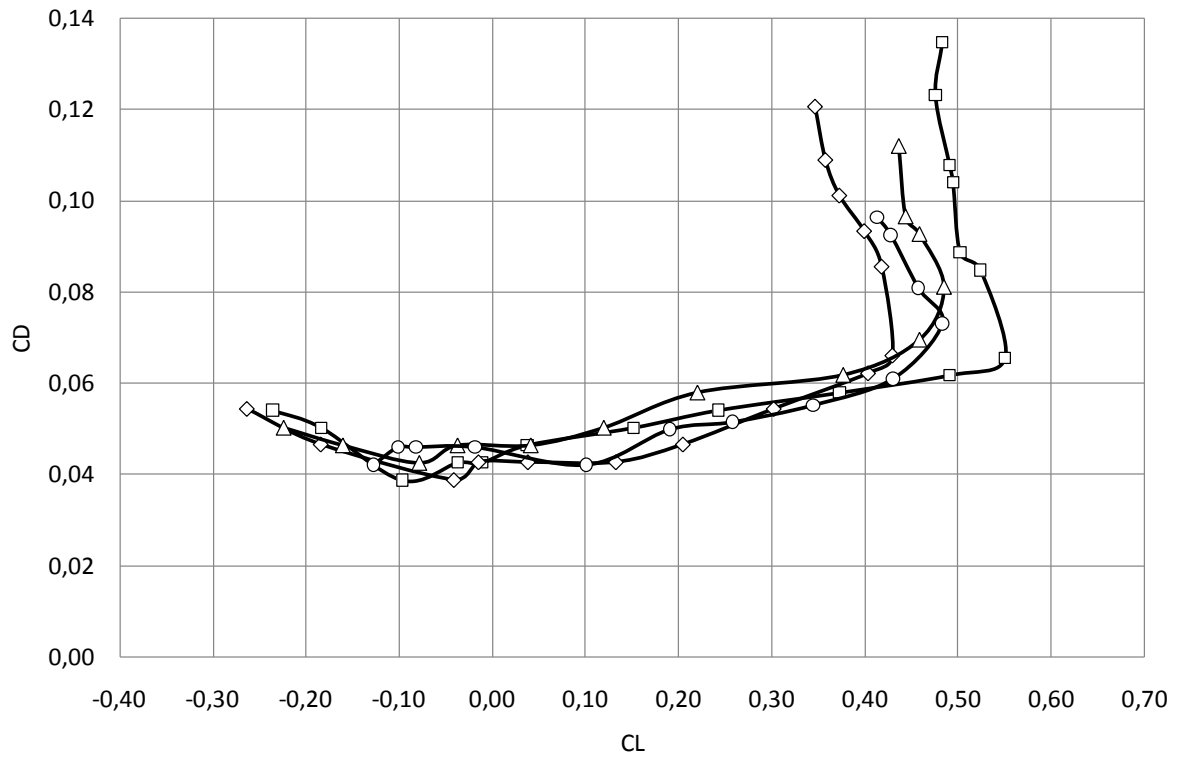


Figure 5.- Variation of drag coefficient (C_D) versus lift coefficient (C_L). The results correspond to $Re=70.000$.

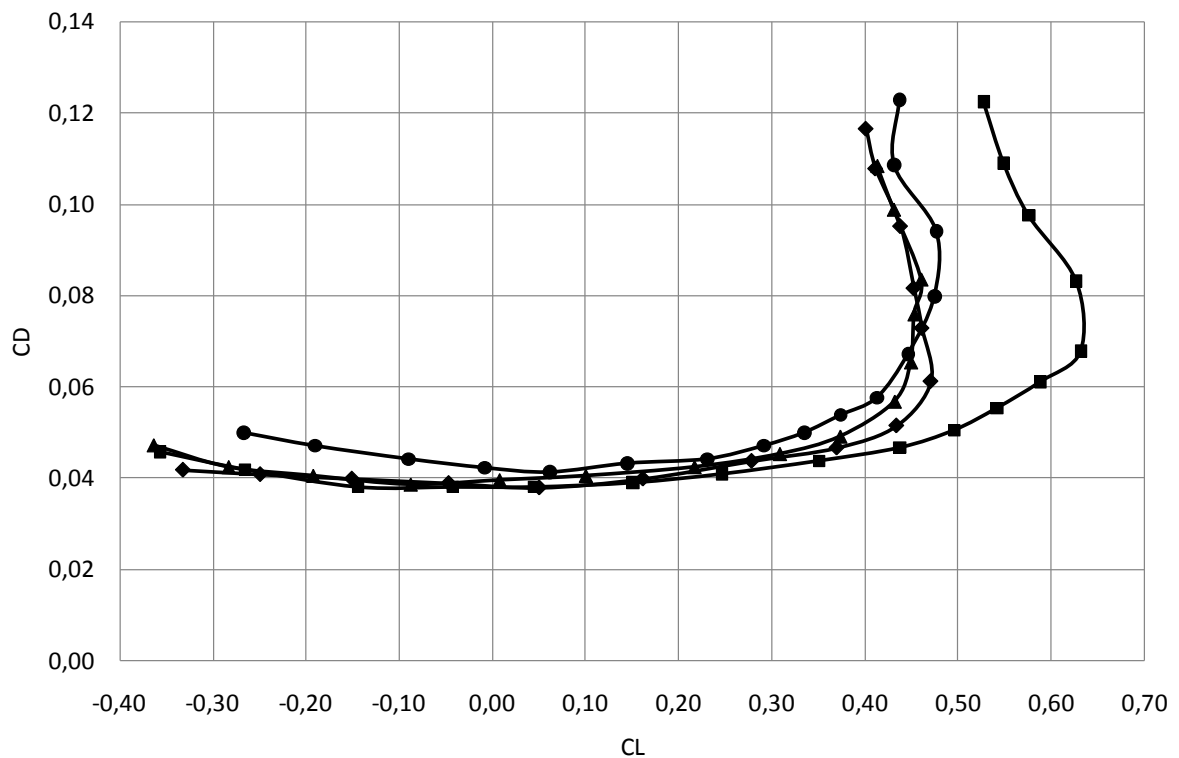


Figure 6.- Variation of drag coefficient (C_D) versus lift coefficient (C_L). The results correspond to $Re=140.000$.

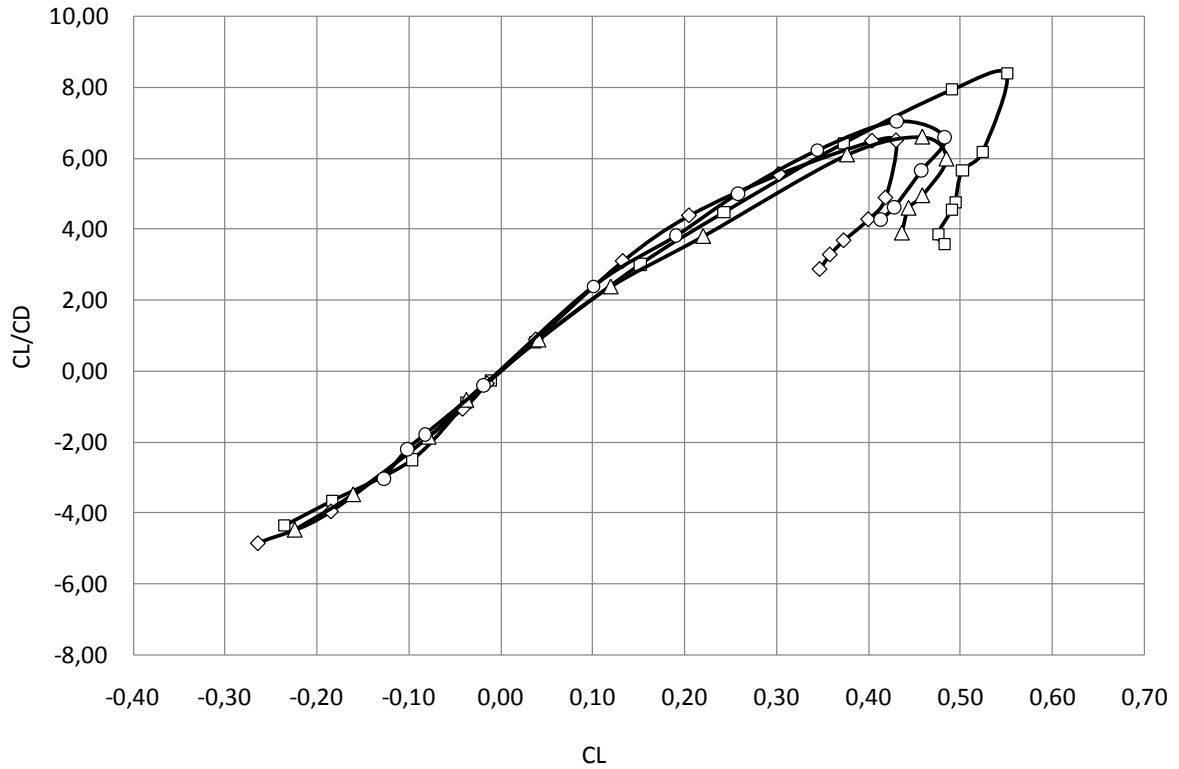


Figure 7.- Aerodynamic efficiency C_L/C_D versus lift coefficient (C_L). The results correspond to $Re=70.000$.

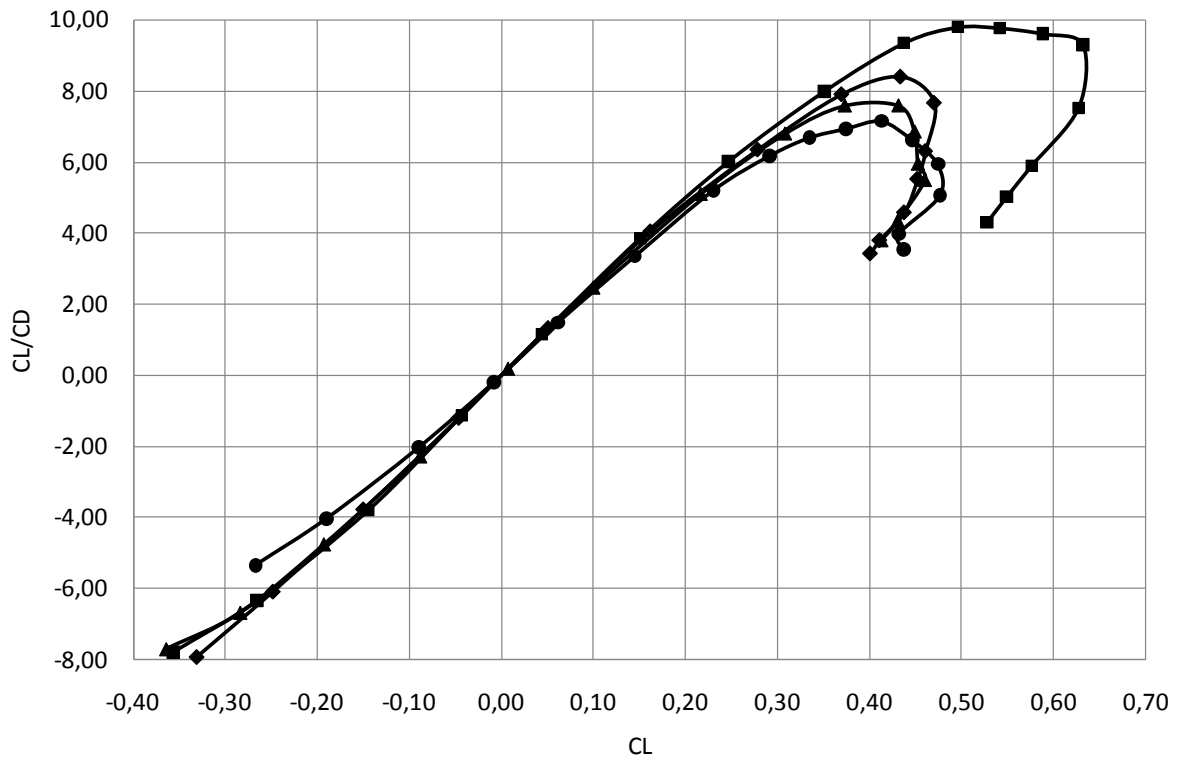


Figure 8.- Aerodynamic efficiency C_L/C_D versus lift coefficient (C_L). The results correspond to $Re=140.000$.

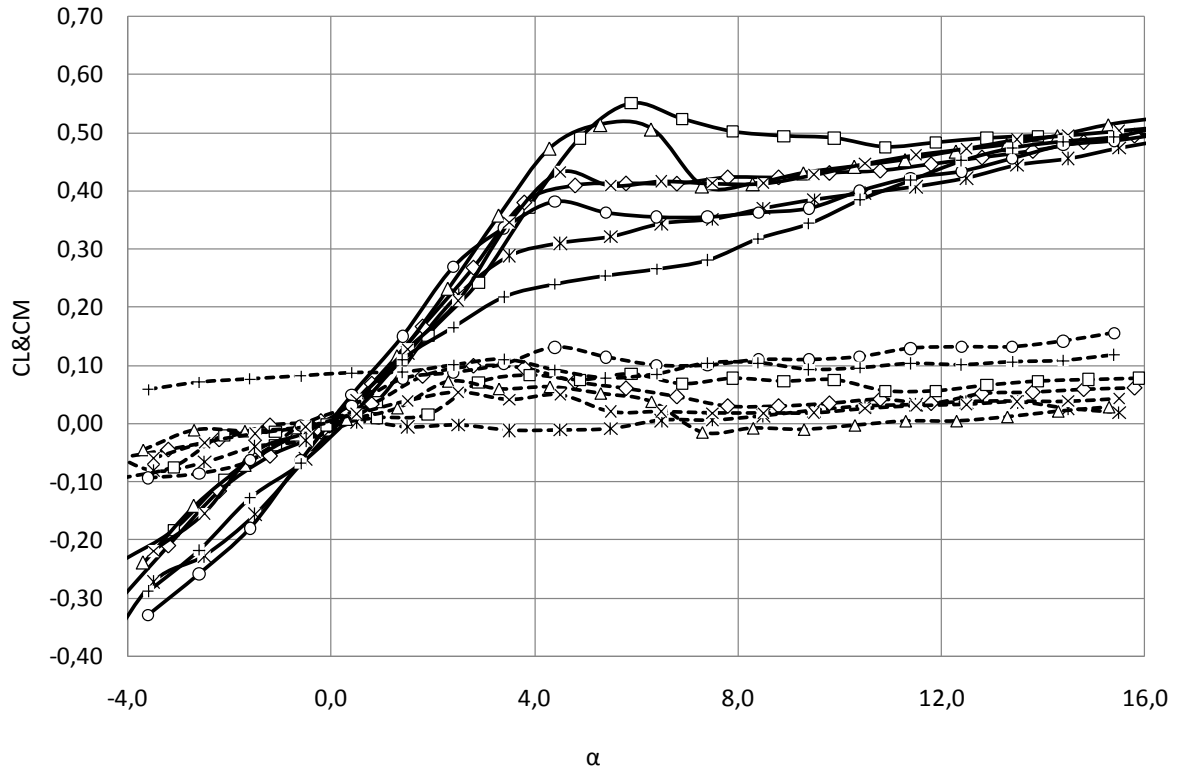


Figure 9.- Variation of lift coefficient (C_L) and pitching moment coefficient (C_M) versus angle of attack (α). The results correspond to $Re= 70.000$.

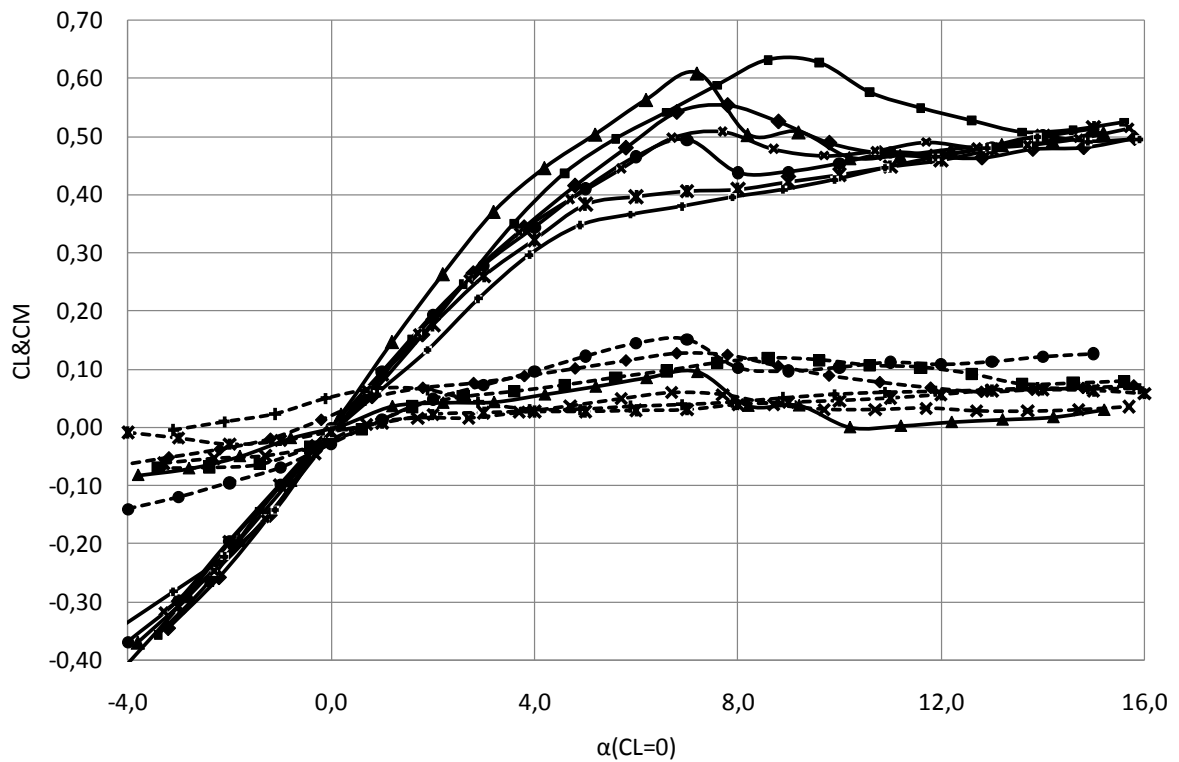


Figure 10.- Variation of lift coefficient (C_L) and pitching moment coefficient (C_M) versus angle of attack (α). The results correspond to $Re= 140.000$.

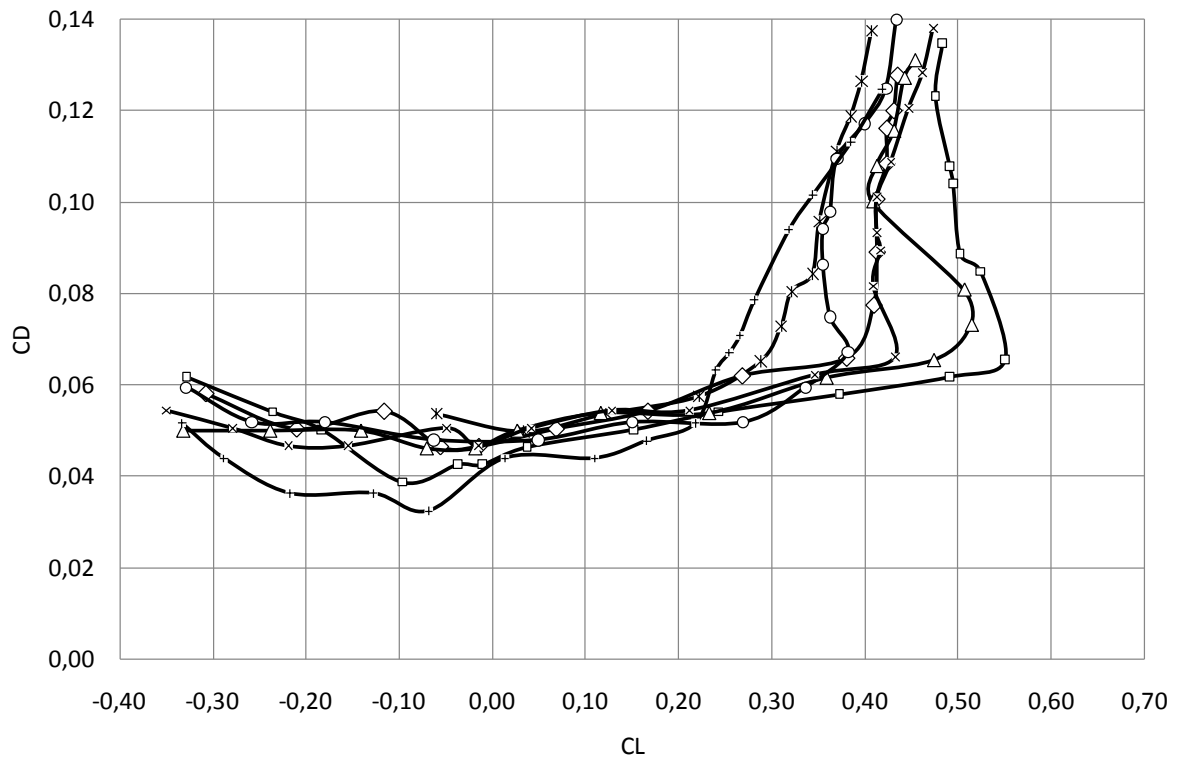


Figure 11.- Variation of drag coefficient (C_D) versus lift coefficient (C_L). The results correspond to $Re= 70.000$.

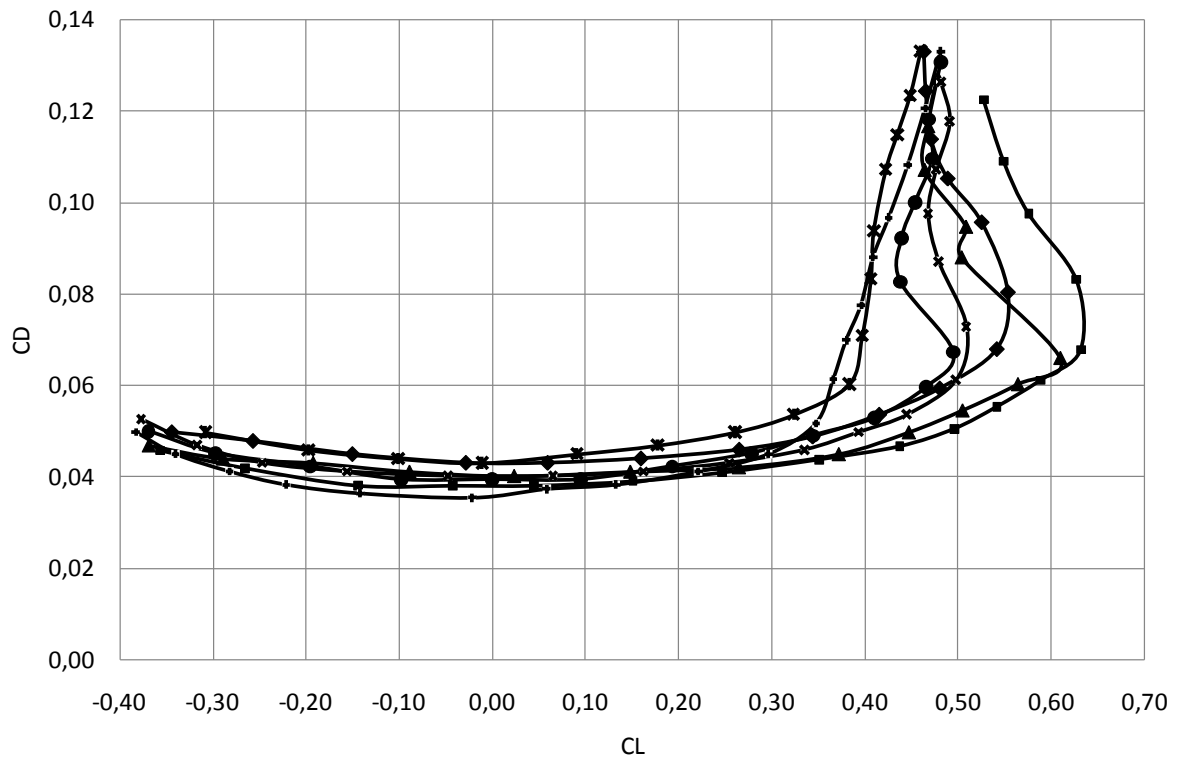


Figure 12.-Variation of drag coefficient (C_D) versus lift coefficient (C_L). The results correspond to $Re= 140.000$.

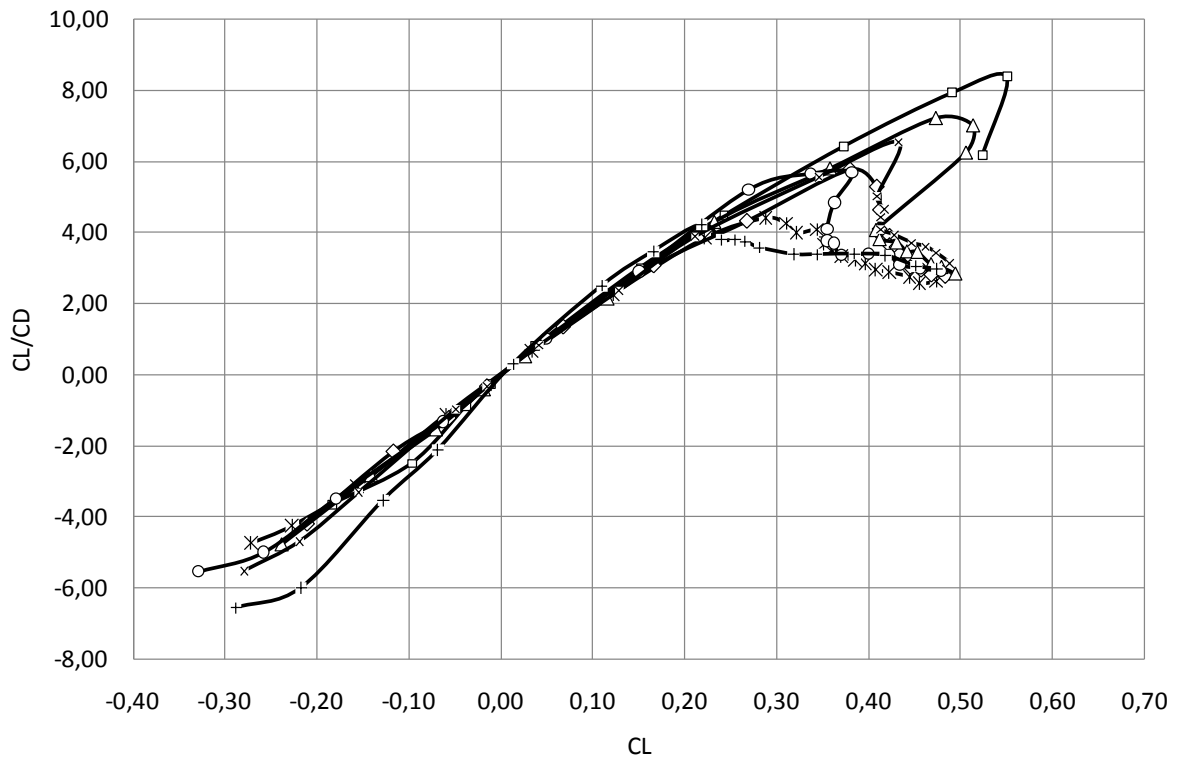


Figure 13.- Aerodynamic efficiency C_L/C_D versus lift coefficient (C_L). The results correspond to $Re= 70.000$.

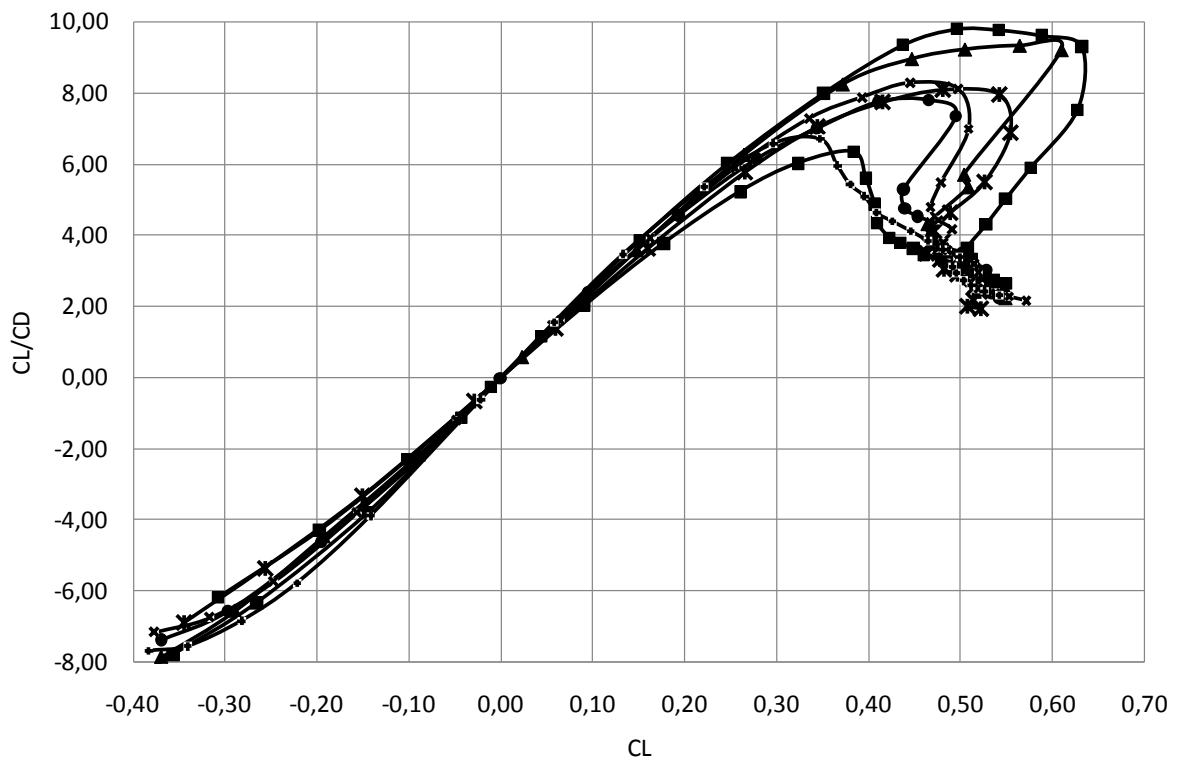


Figure 14.- Aerodynamic efficiency C_L/C_D versus lift coefficient (C_L). The results correspond to $Re= 140.000$.

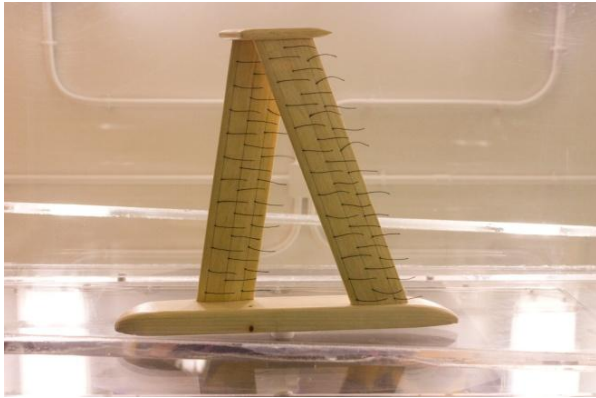


Figure 15. BW2-4 $\alpha= 1^\circ$ (Re=70.000)

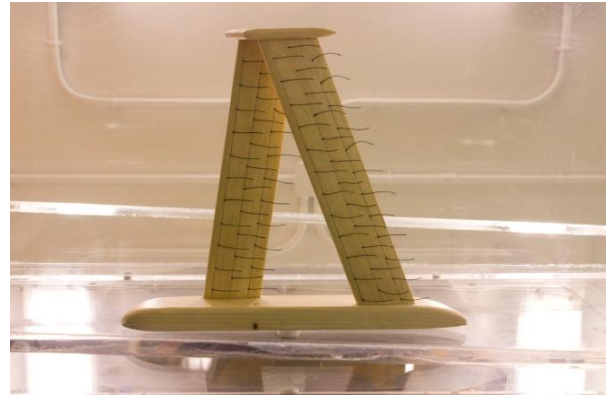


Figure 16. BW2-4 $\alpha= 3^\circ$ (Re=70.000)

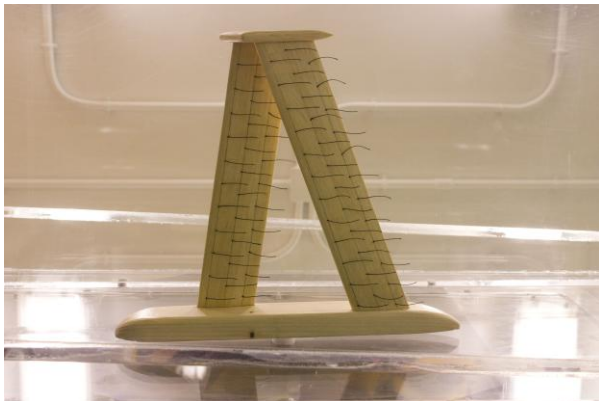


Figure 17. BW2-4 $\alpha= 7^\circ$ (Re=70.000)

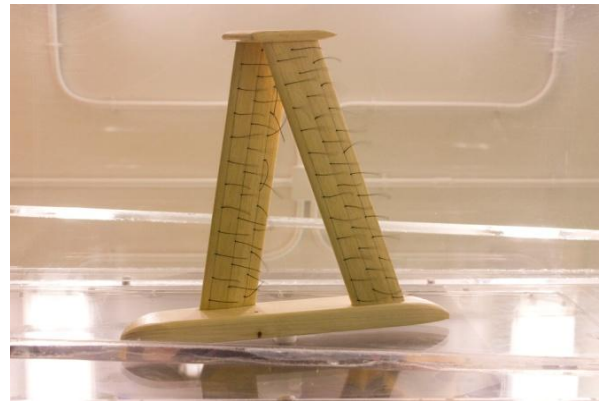


Figure 18. BW2-4 $\alpha= 11^\circ$ (Re=70.000)

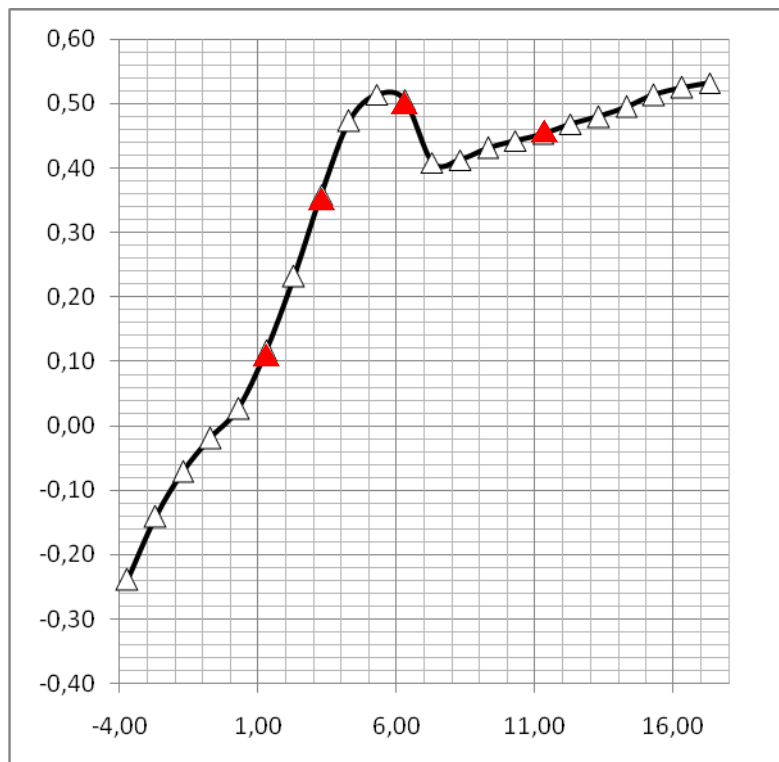


Figure 19.- Lift coefficient (C_L) versus angle of attack (α). The results correspond BW2-4 at Re= 70.000. Symbols identify the box-wing model according to the following key: Corresponding figures 16-19 (close triangles).

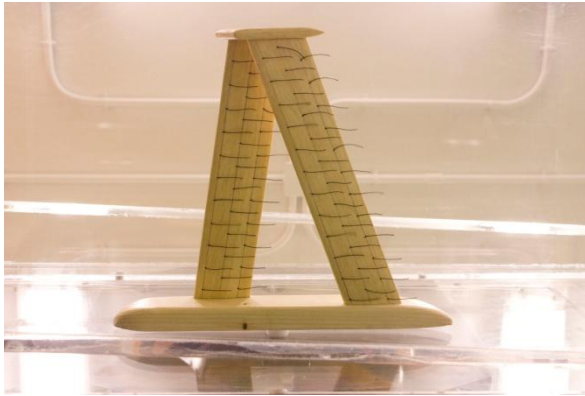


Figure 20. BW2-4 $\alpha = 0^\circ$ (Re=140.000)

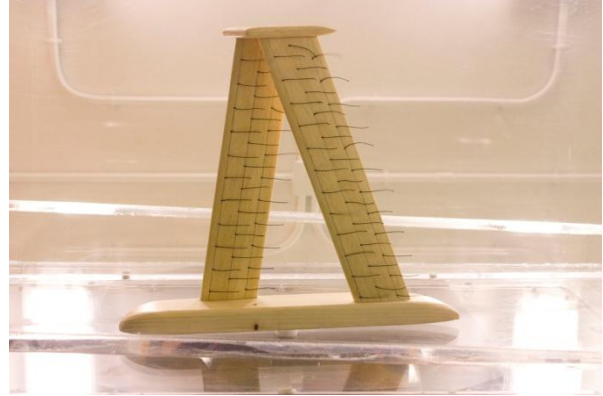


Figure 21. BW2-4 $\alpha = 3^\circ$ (Re=140.000)

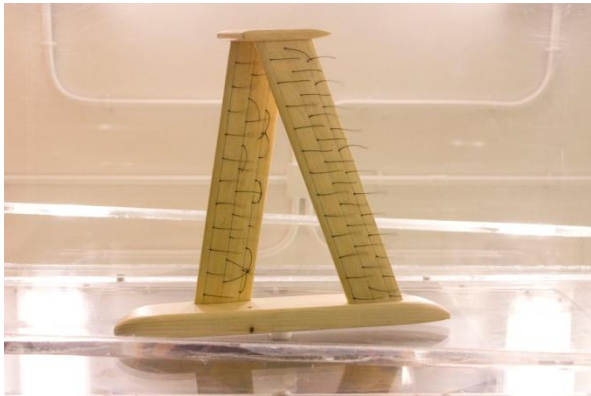


Figure 22.- BW2-4 $\alpha = 6^\circ$ (Re=140.000)

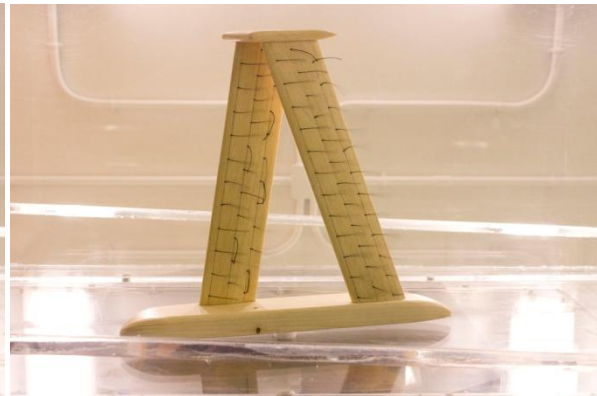


Figure 23.- BW2-4 $\alpha = 11^\circ$ (Re=140.000)

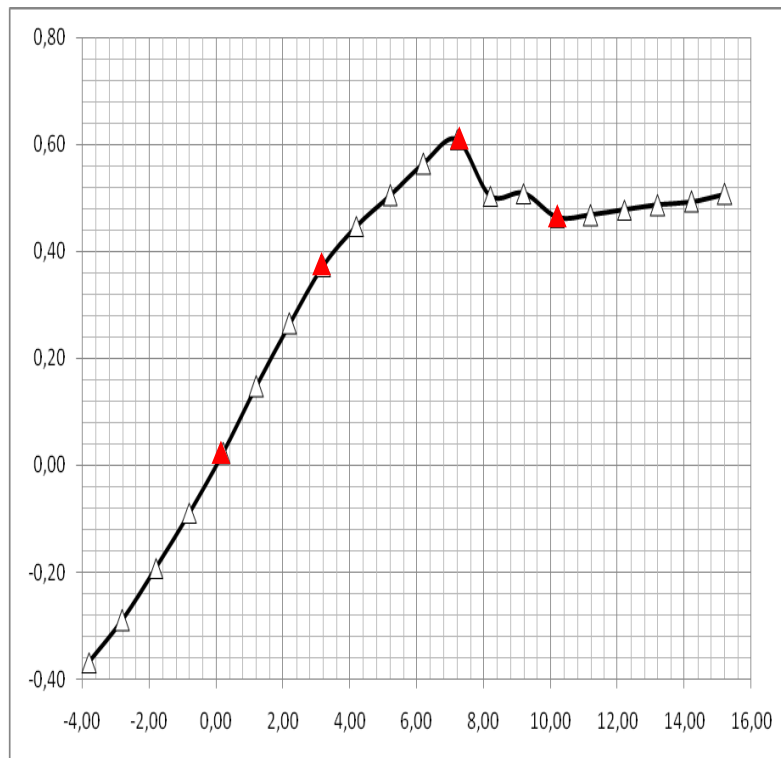


Figure 24.- Lift coefficient (C_L) versus angle of attack (α). The results correspond BW2-4 at Re= 140.000. Symbols identify the box-wing model according to the following key: Corresponding figures 21-24 (close triangles).

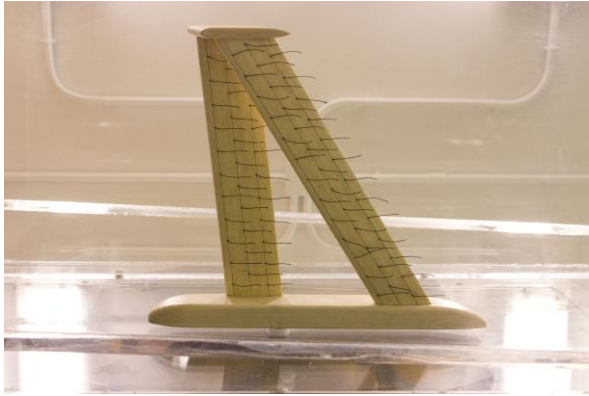


Figure 25.- BW2-6 $\alpha= 0^\circ$ (Re=70.000)

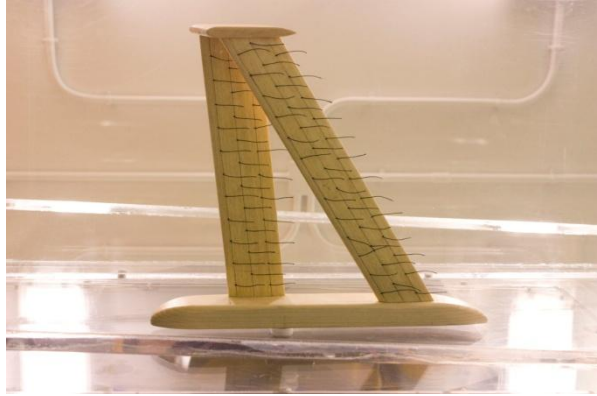


Figure 26.- BW2-6 $\alpha= 3^\circ$ (Re=70.000)

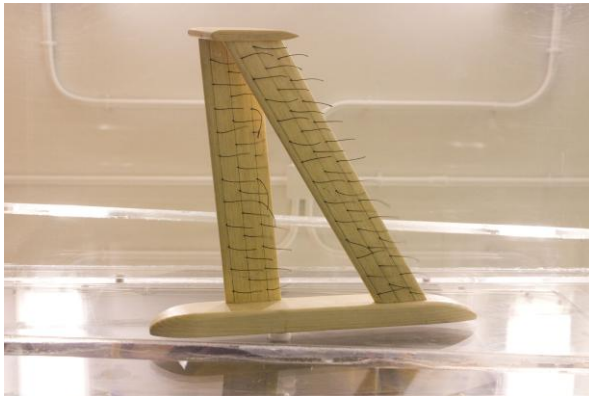


Figure 27.- BW2-6 $\alpha= 6^\circ$ (Re=70.000)

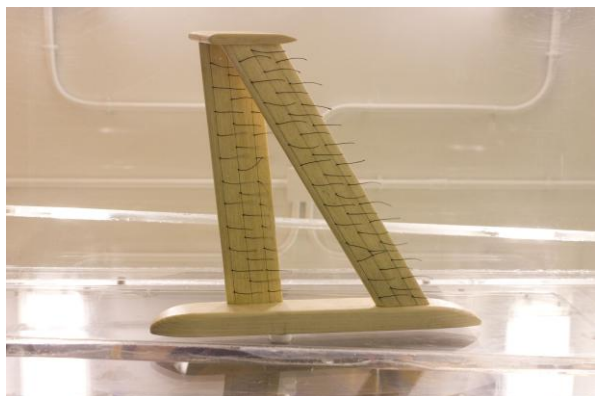


Figure 28.- BW2-6 $\alpha= 11^\circ$ (Re=70.000)

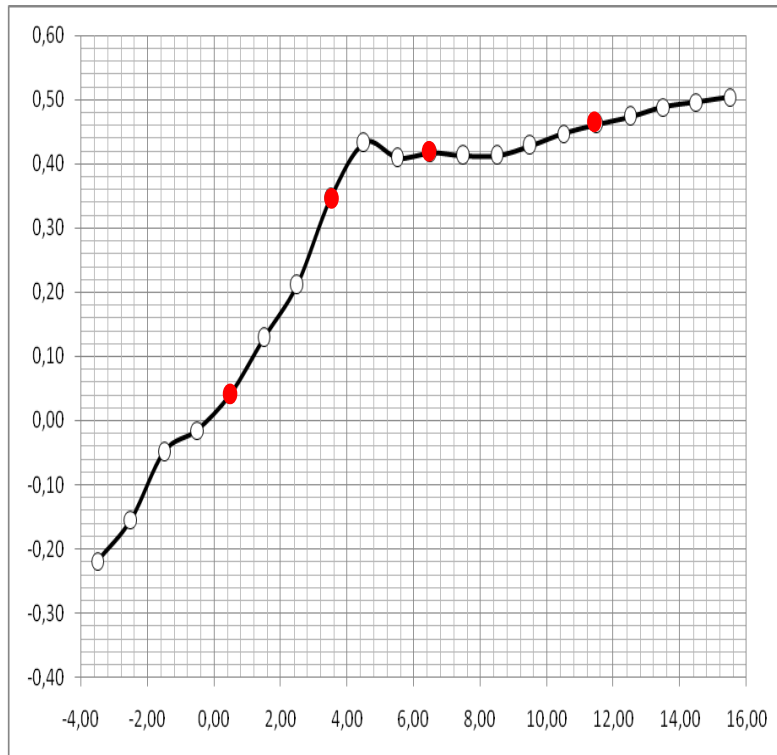


Figure 29.- Lift coefficient (C_L) versus angle of attack (α). The results correspond BW2-6 at Re= 70.000. Symbols identify the box-wing model according to the following key: Corresponding figures 26-29 (close triangles).

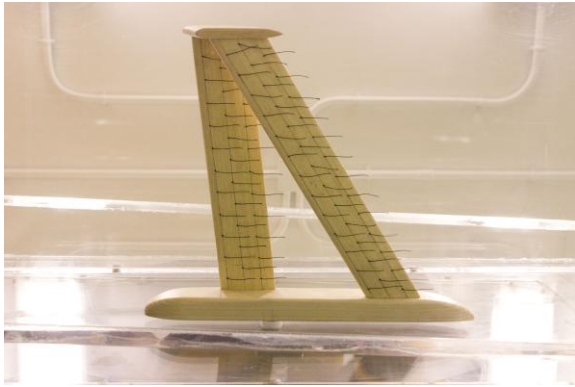


Figure 30.- BW2-6 $\alpha= 1^\circ$ (Re=140.000)

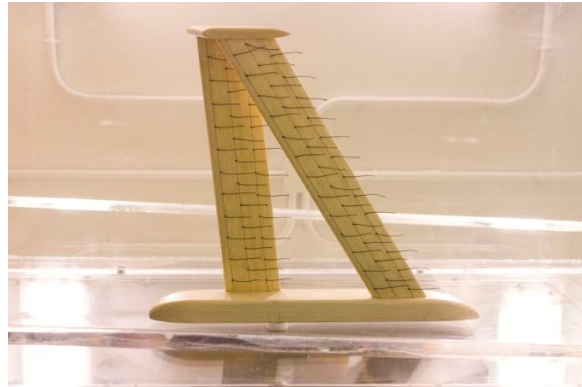


Figure 31.- BW2-6 $\alpha= 4^\circ$ (Re=140.000)

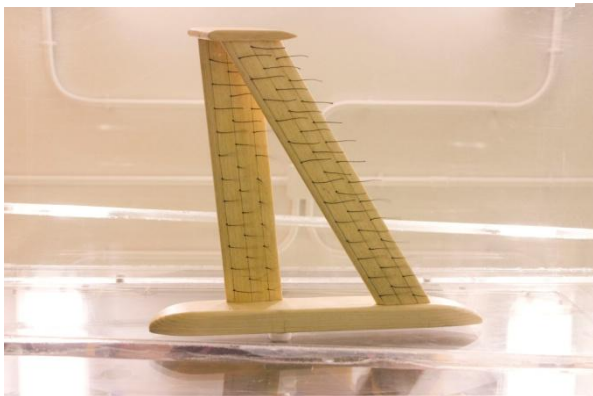


Figure 32.- BW2-6 $\alpha= 8^\circ$ (Re=140.000)

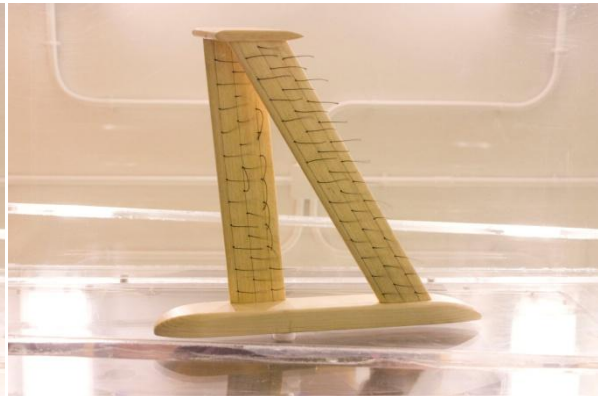


Figure 33.- BW2-6 $\alpha= 12^\circ$ (Re=140.000)

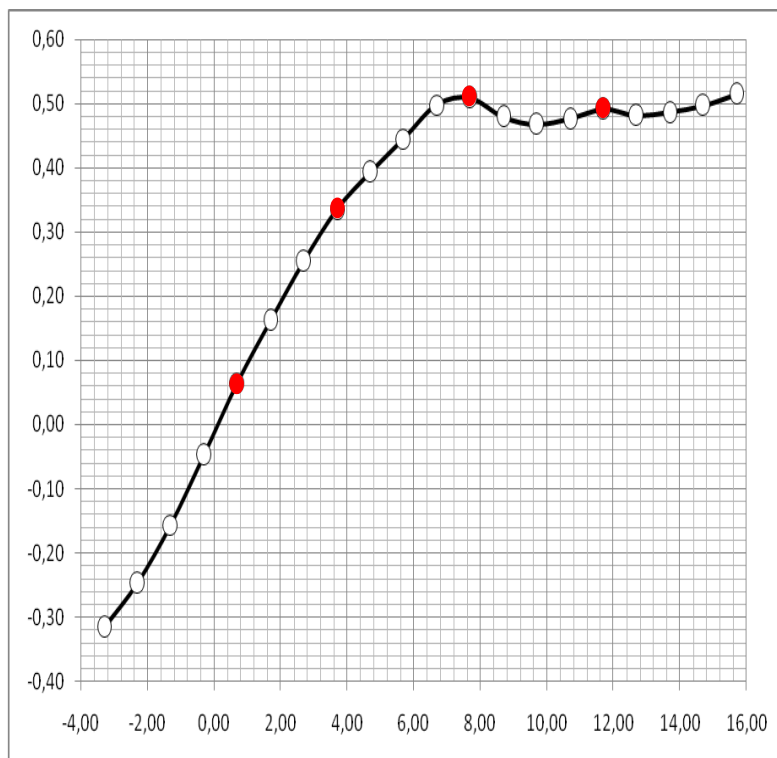


Figure 34.- Lift coefficient (C_L) versus angle of attack (α). The results correspond BW2-6 at Re= 140.000. Symbols identify the box-wing model according to the following key: Corresponding figures 31-34 (close triangles).

References

1. CUERNO-REJADO, C, ALONSO-ALBIR, L., GEHSE, P. Conceptual design of a medium-sized joined-wing aircraft. Proc. IMechE Vol. 224 Part G, Journal of Aerospace Engineering, pp. 681-696, 2010.
2. VIGNERON, Y. Commercial aircraft for the 21st century – A380 and beyond. In Proceedings of the AIAA/ICAS International Air and Space Symposium and Exposition, Dayton, Ohio, USA, AIAA Paper 2003-2886, 2003.
3. TORENBEEK, E. Introductory overview of innovative civil transport aircraft configurations. In: Innovative configurations and advanced concepts for future civil aircraft. Lecture series 2005-2006, (Eds. E. Torenbeek and H. Deconinck), 2005 (von Karman Institute, Brussels, Belgium).
4. PRANDTL, L. Induced drag of multiplanes. NACA TN 182, 1924.
5. FREDIANI, A., RIZZO, E., BOTTONI, C., SCANU, J., CHIAVACCI, L., IEZZI, G. The Prandtlplane aircraft configuration. Aeroday, Wien, 2006.
6. DEL GIUDICE VILLENA, S. Estudio aerodinámico de una aeronave no tripulada del tipo “box-wing” (in Spanish). Final Thesis Report for the Bachelor Degree in Aeronautical Engineering, E.U.I.T. Aeronáutica, UPM, Madrid, September 2010.
7. MARTÍNEZ-VAL R, HERNÁNDEZ C. Preliminary design of a low speed, long endurance RPV for civil applications. Paper No. 3, Proceedings of the 13th Bristol International Conference on RPVs/UAVs, Bristol, UK, 1998.
8. RAYMER, D. P. (1992). Aircraft Design: A Conceptual Approach. Washington, DC: American Institute of Aeronautics and Astronautics, Inc.
9. BARCALA-MONTEJANO, M.A., GANDÍA-AGÜERA, F., RODRÍGUEZ-SEVILLANO, A.A., CRESPO-MORENO, J., PÉREZ-ÁLVAREZ, J., GÓMEZ-PÉREZ, J.P., GÓMEZ-PÉREZ, I. The application of Rapid Prototyping in the design of an UAV. 27th Congress of the International Council of the Aeronautical Sciences (ICAS-2010), Nice-France 19-24 September 2010.
10. BARLOW, J.B., RAE, W.H. POPE. A Low-Speed Wind Tunnel Testing. 3rd ed., John Wiley & Sons, Inc., New York 1999.
11. GALL, P.D. An experimental and theoretical analysis of the aerodynamic characteristics of a biplane-winglet configuration. NASA TM 85815, 1984.